

Article

Compact Ultra-Wideband Bandpass Filters Achieved by Using a Stub-Loaded Stepped Impedance Resonator

Min-Hang Weng ¹, Fu-Zhong Zheng ², Hong-Zheng Lai ² and Shih-Kun Liu ^{2,3,*}¹ School of Information Engineering, Putian University, Putian 351100, China; hcwweng@gmail.com² Institute of Photonics Engineering, National Kaohsiung University of Science and Technology, Kaohsiung 80778, Taiwan; 1098319123@nkust.edu.tw (F.-Z.Z.); f107155102@nkust.edu.tw (H.-Z.L.)³ Doctoral Degree Program in Biomedical Engineering, Kaohsiung Medical University, Kaohsiung 80708, Taiwan

* Correspondence: skliu@nkust.edu.tw

Received: 3 January 2020; Accepted: 19 January 2020; Published: 22 January 2020



Abstract: In this paper, we develop a bandpass filter using a stub-loaded stepped impedance resonator (SLSIR) and calculate the even and odd resonant modes of this type of resonator using the input impedance/admittance analysis. In this study, two impedance ratios and two length ratios are operated as the design parameters for controlling the resonant modes of the SLSIR. Several resonant mode variation curves operating three resonant modes with different impedance ratios and two length ratios are developed. By tuning the desired impedance ratios and length ratios of the SLSIRs, compact ultra-wideband (UWB) bandpass filters (BPFs) can be achieved. Two examples of the UWB BPFs are designed in this study. The first example is UWB filter with a wide stopband and the second one is dual UWB BPF, namely, with UWB performance and a notch band. The first filter is designed for a UWB response from 3.1 to 5.26 GHz having a stopband from 5.3 to 11 GHz, with an attenuation level better than 18 dB. The second filter example is a dual UWB BPF with the frequency range from 3.1 to 5 GHz and 6 to 10.1 GHz using two sets of the proposed SLSIR. The measured results have insertion loss of less than 1 dB, and return loss greater than 10 dB. Furthermore, the coupling structures and open stub of the SLSIR also provide several transmission zeros at the skirt of the passbands for improving the passband selectivity.

Keywords: ultra-wideband; bandpass filter; stub-loaded; stepped impedance resonator

1. Introduction

The Federal Communication Commission (FCC) proposed ultra-wideband (UWB) to solve the problem of data transmission. This frequency ranges from 3.1 to 10.1 GHz. Typically, the range of operational frequency of ultra-wideband is divided into two sections: one section from 3.1 to 5 GHz, the other is from 6 to 10.1 GHz. A notch band appears at 5 to 6 GHz in the UWB from 3.1 to 10.1 GHz to avoid interfering with the signal of the popular wireless local area network (WLAN) [1].

A bandpass filter (BPF) is an essential part of the front end of wireless communications. Thus, UWB BPF is increasingly popular and has been extensively developed [2–24]. In [2,3], dual-mode ring resonators were used to obtain the UWB BPFs with controllable bandwidth adjusted by the feeding position. In [4], a mode-excited resonator was used to develop a UWB BPF with an extremely broad stopband. In [5], cross-shaped resonator was used for a UWB bandpass filter having a sharp skirt and notched band. In [6,7], a UWB BPF with a wide stopband was proposed by using defected ground structure (DGS). In [8,9], parallel coupled lines were developed to have wideband filter responses with high selectivity. In [10], transmission lines implemented on metamaterial-inspired co-planar waveguide (CPW) balanced cells were utilized to obtain wideband performance. Moreover, in [11],

multiple-mode split-ring resonators in a rectangular waveguide cavity were realized to achieve a wideband BPF design. However, most of above designs suffer from decreased design freedoms to tune the bandwidth and band selectivity.

Recently, multiple-mode resonator (MMR) have become commonly used as basic building blocks for wideband BPFs. Especially, stepped-impedance resonator (SIR) and stub-loaded resonator (SLR) are two most-general MMRs. The standard SIR is symmetrical structure with non-continuous impedance shaped like a dumbbell. SIR can adjust the harmonics by changing the length ratio and impedance ratio to achieve multiband or wideband performance. In [12], asymmetric SIR was used to achieve a compact UWB BPF having good band selectivity and wide stopband performance. In [13], an embedded SIR was used to achieve wideband response with a notch band. SLR structures are typically categorized into two types: open ended and short ended. In most SLR structures, the fundamental resonant frequency is determined by the main resonator and the other higher frequencies can be determined by adjusting the stub. The combination of the conventional resonator with the stub load able to have more design freedoms. In [14–16], stub-loaded multiple-mode resonators were employed to obtain UWB BPF with improved in-band performance. Moreover, in [17,18], stepped-impedance stub-loaded resonator (SISLR) was presented to have more design parameters to control the wideband responses such as bandwidth and selectivity. In [18,19], a quadruple mode ring resonator and penta-mode resonator was presented to achieve sharp-rejection broadband BPF. In [20–24], various types of stub-loaded resonators such as C-shaped and E-shaped resonators, and multi-layered substrate with two stub-loaded resonators were developed to design UWB BPF with notched bands to have high band selectivity. In previous studies, SIR combined with an open stub load was implemented to obtain dual- [25] and tri-band BPFs [26]. However, the analysis of the SIR combined with an open stub load was not described in detail.

In this paper, a stub-loaded stepped impedance resonator (SLSIR) is developed, as shown in Figure 1. The developed SLSIR was constructed from a conventional two-step SIR added with an open circuited stub at the symmetry line of the SIR. It is well known the SIR will shift the higher order modes far away or near the fundamental mode as the impedance ratio becomes larger than 1 or less than 1 [27]. The input impedance/admittance analysis is employed to obtain the even and odd resonant modes of this type of resonator in detail. For controlling the resonant modes of the SLSIR, two impedance ratios and two length ratios can be used as the design parameters. By using the impedance/admittance analysis, several variation curves with all possible resonant modes are obtained. Two types of compact UWB BPFs are designed by applying only the SLSIR with tuning of the desired impedance ratios and length ratios. In the first filter example, a UWB filter with a wide stopband filter is designed. The first odd mode and even mode constitute a UWB response from 3 to 5.1 GHz, and the other modes are shifted to far away from the passband to form a wide stopband with an attenuation better than -18 dB from 5.9 to 12 GHz. The passband edge has three transmission zeros, making high attenuation and isolation. In the second filter example, a dual ultra-wideband BPF is designed. The first odd mode and even mode in the proposed resonator constitute a passband of the ultra-wideband. Therefore, the result of the passband can be expected. The passband edge of the filter has five transmission zeros, also providing a good attenuation and isolation. This paper is organized as follows: The introduction section describes the background, motivation and novelty of this study. Several design methods of the UWB BPF are reviewed; the second section analyzes the SLSIR and develops several resonant mode variation curves of SLSIR; the third section describes the design of UWB filter with a wide stopband; the fourth section describes the design of dual UWB filter (namely, a UWB with a notch band). Two filter examples were fabricated, and the measured results are found to be in good agreement with the simulated results. In conclusion, the benefits and new discovery of this design are made and addressed.

2. Analysis of the SLSIR

Figure 1 shows the structure of the SLSIR which first appeared in [10]. However, the structure is only used to design a dual-band filter. The reported design is the simulated result without accompanying theoretical analysis.

In this paper, theoretical analysis for the structure is orderly executed by the transmission line theory. In Figure 1a, the Z_1 , Z_2 and Z_S denote the particular characteristic impedance of the stepped impedance resonator and the open stub, and θ_1 , θ_2 and θ_S represent the electronic length of the stepped impedance resonator and the open stub, respectively.

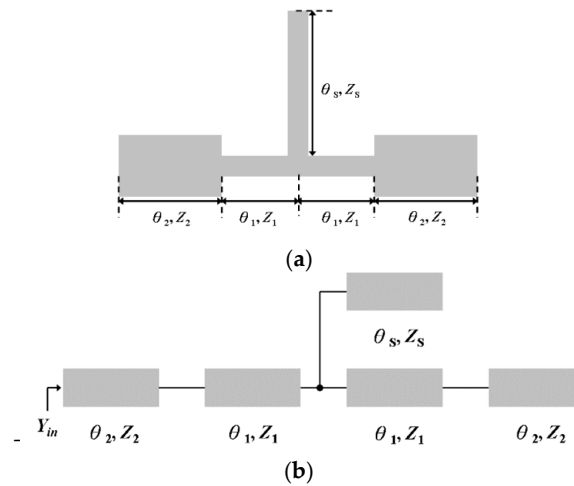


Figure 1. (a) The structure and (b) the equivalent block of the proposed stub-loaded stepped impedance resonator.

The structure of the SLSIR is mirror symmetry, and it has six variables to be controlled. Figure 1b is the equivalent block of the SLSIR. The input admittance (Y_{in}) can be calculated by transmission line theory as the following [28]:

$$Y_{in} = \frac{1}{Z_2} \frac{Z_1(K_1 - \tan \theta_1 \tan \theta_2) + jZ_L(K_1 \tan \theta_1 + \tan \theta_2)}{Z_L(1 - K_1 \tan \theta_1 \tan \theta_2) + jZ_1(\tan \theta_1 + K_1 \tan \theta_2)} \quad (1)$$

where $Z_L = \frac{jZ_1K_2(\tan \theta_1 \tan \theta_2 - K_1)}{K_2(\tan \theta_2 + K_1 \tan \theta_1) - \tan \theta_s(\tan \theta_1 \tan \theta_2 - K_1)}$; $K_1 = \frac{Z_2}{Z_1}$; $K_2 = \frac{Z_S}{Z_1}$

K_1 and K_2 are two defined impedance ratios, regarding to the SIR and stub, respectively. The resonant modes of the formula are derived by setting Y_{in} equal to zero, as following [29]:

$$(K_1 - \tan \theta_1 \tan \theta_2) = 0 \quad (2)$$

and

$$[2K_2(K_1 \tan \theta_1 + \tan \theta_2) + \tan \theta_s(K_1 - \tan \theta_1 \tan \theta_2)] = 0 \quad (3)$$

It is shown Equations (2) and (3) are related to the odd- and even-mode resonances of the SLSIR, respectively. Since there are three electronic lengths θ_1 , θ_2 and θ_S in the formula, two other length ratios can be defined to gain more design freedom. The first length ratio (R_1) of the SIR is defined as $R_1 = 2\theta_2/2(\theta_1+\theta_2) = 2\theta_2/\theta_T$ and the second length ratio (R_2) of the stub with SIR is defined as $R_2 = 2\theta_S/\theta_T$, where θ_T is the total length of the SIR section defined as $2(\theta_1+\theta_2)$, and θ_S is the length of the stub. Thus, R_1 and R_2 can also be varied to tune the higher order resonant modes in a wide frequency range. Thus, by setting the length ratio (R_1) and the length ratio (R_2) into Equations (2) and (3), resonant modes of the proposed can be controlled by four varied parameters, (K_1 and K_2) and (R_1 and R_2).

Figure 2 shows the length ratio R_1 with resonant electric length θ_T using MATLAB at various length ratios, $R_2 = 0.1, 0.3, 0.5, 0.7$ and 0.9 . Z_s is set to be equal to Z_1 , i.e., $K_2 = 1$ to reduce the plot complexity.

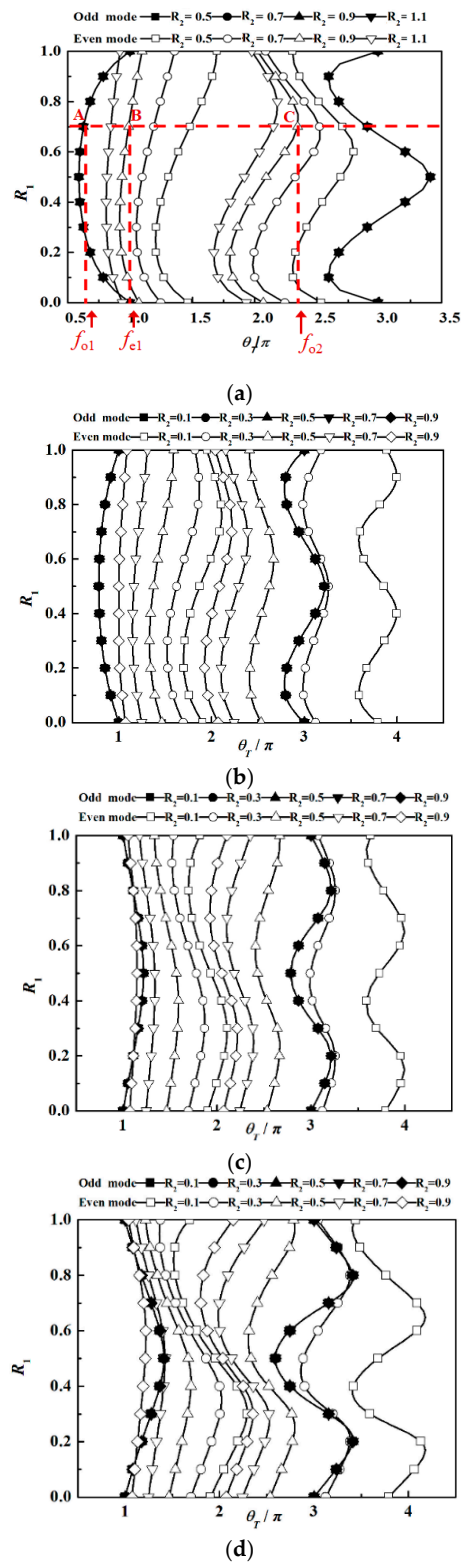


Figure 2. Length ratio R_1 with resonant electric length θ_T using the MATLAB tool at various length ratios, $R_2 = 0.1, 0.3, 0.5, 0.7$ and 0.9 based on (a) $K_1 = 0.25$ and $K_2 = 1$, (b) $K_1 = 0.5$ and $K_2 = 1$, (c) $K_1 = 2$ and $K_2 = 1$ and (d) $K_1 = 4$ and $K_2 = 1$.

As shown in Figure 2, multi-resonant modes are varied as four parameters. It is clearly found that the length ratio R_2 would not affect the resonances of the odd modes since the stub is ignored under the odd mode excitation; and the length ratio R_2 affects the resonances of the even mode obviously. The fundamental odd mode shifts to lower frequency for $K_1 < 1$ (shown in Figure 2a,b) and to higher frequency for $K_1 > 1$ (shown in Figure 2c,d), as similar to the conventional SIR. Especially, in the condition of $K_1 > 1$, at the lowest resonant frequency the even and odd modes of the proposed SLSIR join together, indicating different behavior from the resonant modes of the typical SIR. Therefore, by using these resonant curves, the structure can be designed for the different filters, for example dual-band BPF, tri-band BPF, UWB BPF and wide stopband BPF, by controlling the multi-resonant modes.

In this study, two types of UWB BPFs are designed by applying the SLSIR by tuning the desired impedance ratios and length ratios.

3. UWB BPF with Wide Stopband

In the first example, a UWB BPF with a wide stopband filter is presented. Figure 3 shows the structure of the designed filter. It mainly comprises a SLSIR with input/output coupled lines. The required passband of this BPF is set from 3.1 to 5.2 GHz, where the stopband is designed from 5 to >10 GHz.

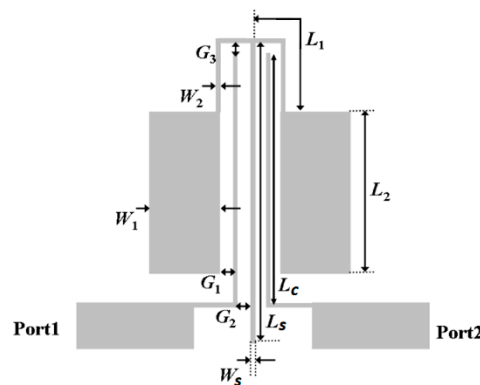


Figure 3. Structure of the ultra-wideband bandpass filter with a wide stopband.

3.1. Design Procedure

For achieving the required specification, the first odd mode and even mode are selected to constitute a UWB response from 3 to 5.2 GHz, and the other modes shall be shifted to far away from the passband to form a wide stopband. In this study, $K_1 = 0.25$ and $K_2 = 1$, as the mapping in Figure 2a is used. In this design, the first even mode (f_{e1}) and odd mode (f_{o1}), as shown in spot A and spot B in Figure 2a respectively, are set to form the UWB response. The desired resonant frequencies of the SLSIR are set as: $f_{o1} = 3.1$ GHz and $f_{e1} = 4.8$ GHz. For a wide stopband, f_{o2} is set to be greater than 10 GHz, as shown in spot C in Figure 2a. Namely, the passband frequency ratios f_{e1}/f_{o1} is 1.55 and f_{o2}/f_{o1} greater than 3.2 is required. There would be many solutions to satisfy the required conditions, thus many groups (R_1, R_1) can be selected in various groups (K_1, K_2). As mapping in Figure 2a, the corresponding length ratio R_1 is found to be 0.7 and length ratio R_2 is found to slightly more than 0.9, where the passband frequency ratios of $f_{e1}/f_{o1} = 1.58$ and f_{o2}/f_{o1} is greater than 4.64.

Both of the high impedance Z_1 and Z_S are set to be 152Ω , and thus the low impedance Z_2 is set to be 38Ω . According to Figure 2a, the electrical length θ_1 , θ_2 , and θ_S are decided as 22° , 50° , and 113° , respectively. Thus, the structure parameters of the SLSIR are obtained as: $L_1 = 3.35$ mm, $L_2 = 7.1$ mm, $L_s = 13.7$ mm, $W_1 = 3.38$ mm, $W_2 = 0.2$ mm, $W_s = 0.2$ mm. In order to miniaturize the filter size, the proposed SLSIR is folded and the input coupled line and output coupled line with high impedance are inserted into the SLSIR, as shown in Figure 3, to have an enough coupling. Therefore, the first even modes (f_{e1}) and odd modes (f_{o1}) can be coupled together to form the UWB. Figure 4 displays

the simulated results of the UWB filter with a wide stopband using a full wave electromagnetic (EM) simulation [30]. When setting $G_1 = 0.2$ mm, $G_2 = 0.15$ mm and $G_3 = 0.15$ mm, the simulated insertion loss $|S_{21}|$ and return loss $|S_{11}|$ are around 0.56 dB and 14.9 dB respectively. Further, the 3-dB fractional bandwidth (FBW) is about 53.0%, and the wide stopband is from 5.9 to 11 GHz with an attenuation larger than -18 dB.

The proposed filter has the advantage of the appearance of the transmission zeros, which are produced by the open stub (L_s) and the coupling length (L_c) of the I/O lines. The length of the open stub is represented as L_s , and the length of the coupling surface is represented as L_c . The transmission zeros of the filter generated by the L_s is expressed as [29]

$$f_Z = (2n - 1)f_0 \frac{\lambda_g}{4 \times L_s} \quad (n = 1, 2, 3, \dots) \quad (4)$$

The transmission zeros of the filter generated by the L_c is expressed as [29]

$$f_Z = (n - 1)f_0 \frac{\lambda_g}{4 \times L_c} \quad (n = 1, 2, 3, \dots) \quad (5)$$

where f_0 is the center frequency and λ_g is the guided wavelength corresponding to the center frequency. With $L_s = 13.7$ mm and $L_c = 11.9$ mm, the expected transmission zeros are calculated to be 2.48 GHz (TZ₁) by using Equation (4), and the transmission zeros are determined to be 2.90 GHz (TZ₂) and 5.95 GHz by (TZ₃) using Equation (5). The passband edge has three transmission zeros, making a good band selectivity, as shown in Figure 4.

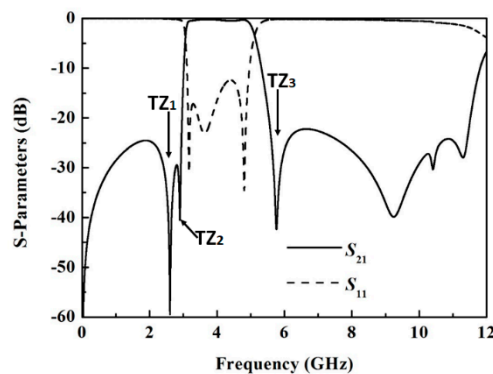


Figure 4. Simulated results of the UWB filter with a wide stopband using EM simulation. $L_1 = 3.35$ mm, $L_2 = 7.1$ mm, $L_s = 13.7$ mm, $L_c = 11.9$ mm, $W_1 = 3.38$ mm, $W_2 = 0.2$ mm, $W_s = 0.2$ mm, $G_1 = 0.2$ mm, $G_2 = 0.15$ mm, $G_3 = 0.15$ mm.

3.2. Measured Results

The designed filter is realized on 0.787 mm thick substrate (RT/Duroid 5880) having a dielectric constant and a loss tangent of 2.2 and 0.0009, respectively. The filter is optimized using a full wave EM simulation [30] and the dimension parameters are: $L_1 = 3.35$ mm, $L_2 = 7.1$ mm, $L_s = 13.7$ mm, $W_1 = 3.38$ mm, $W_2 = 0.2$ mm, $W_s = 0.2$ mm, $G_1 = 0.2$ mm, $G_2 = 0.15$ mm, $G_3 = 0.15$ mm.

Figure 5a shows a photograph of the fabricated BPF. The overall size of this BPF is about 10 mm \times 20 mm, around $0.15 \lambda_g \times 0.25 \lambda_g$, where λ_g is the guided wavelength at the center frequency. Figure 5b displays the simulated and measured results of the designed UWB BPF with a wide stopband. For the measurement, an HP 8510C network analyzer was used after first being calibrated. The measured results have average insertion loss $|S_{21}|$ of 0.94 dB, average return loss $|S_{11}|$ of 16.2 dB and 3-dB fractional bandwidth (FBW) = 52.7%. The transmission zeros appeared near the passband at 2.5 GHz (TZ₁), 2.95 GHz (TZ₂) and 6.1 GHz (TZ₃), thus having a high isolation. The measured group delay has a small varying range from 0.2 ns to 0.4 ns. Although the simulated results and the measured

results have a slight mismatch in the high frequency region, this is typically caused due to the material limitation of the substrate. The filter has a simple structure and good filter features, thus it has a good potential to be applied in UWB applications.

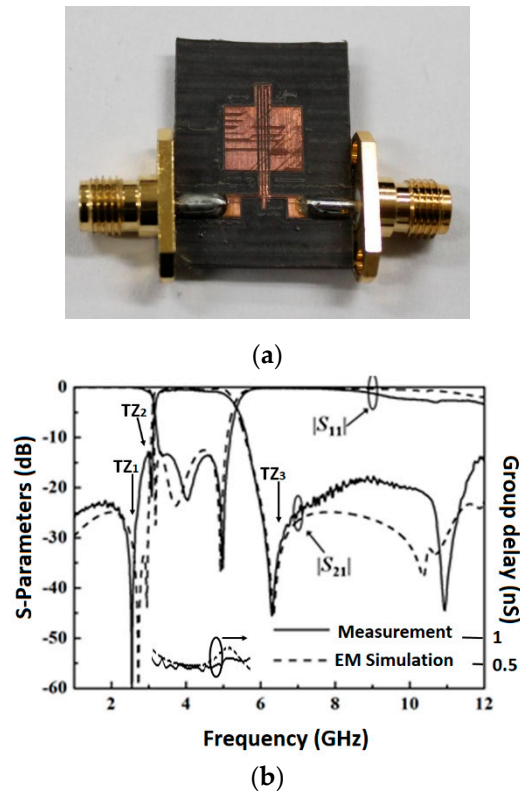


Figure 5. (a) Photograph and (b) simulated and measured results of the BPF with a wide stopband. $L_1 = 3.35$ mm, $L_2 = 7.1$ mm, $L_s = 13.7$ mm, $W_1 = 3.38$ mm, $W_2 = 0.2$ mm, $W_s = 0.2$ mm, $G_1 = 0.2$ mm, $G_2 = 0.15$ mm, $G_3 = 0.15$ mm.

4. Design of Dual UWB Bandpass Filter

In the second design example, a dual ultra-wideband BPF is presented. Figure 6 shows the configuration of the dual UWB BPF. This filter combines two UWB BPFs based on the above work of section III. The upper SLSIR is used to form the first UWB BPF with 3.1 to 5 GHz and the lower SLSIR is used to form the second UWB BPF with 6 to 10.2 GHz. Before combining the first UWB BPF and the second UWB BPF, they are designed independently to match the requirements of the first and second UWB responses. As addressed above, in the used SLSIR, the first odd mode and first even mode constitute together a passband of the ultra-wideband. The passband edge of filter has five transmission zeros, also providing a good attenuation and isolation. Moreover, the designed dual UWB BPF can be seen as a UWB BPF with a notch band.

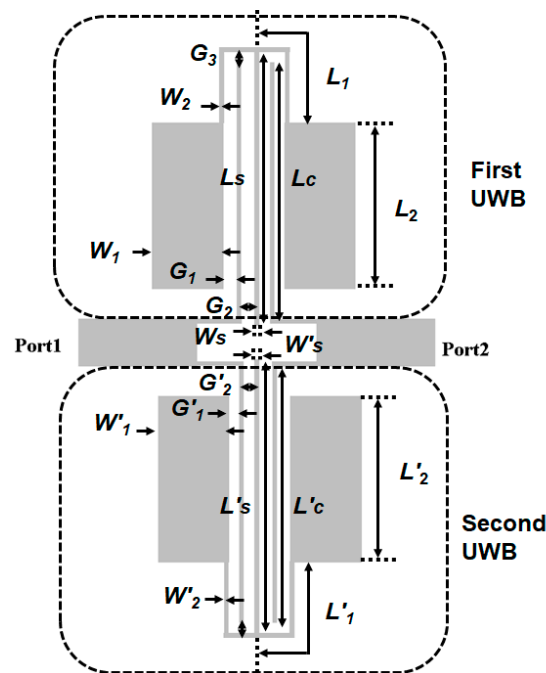


Figure 6. Configuration of the dual UWB BPF.

4.1. Design Procedure

The first UWB response is set from 3.1 to 5 GHz with a stopband from 5.5 to >11 GHz, as in Section 3. The designed UWB BPF with a wide stopband is optimized using the EM simulation [30] and the dimension parameters are shown in Figure 4. The simulated results have a wide stopband with an attenuation is larger than 20 dB from 5.9 to 12 GHz, as shown in Figure 4. Therefore, the second UWB response can be designed in the wide stopband region of the first UWB response.

The second UWB response is thus set from 6 to 10.1 GHz. Using the same structure as shown in Figure 4, the desired resonant frequencies of the SLSIR are set as: $f_{o1} = 6$ GHz and $f_{e1} = 9.3$ GHz. Namely, the passband frequency ratio f_{e1}/f_{o1} is 1.55. Similarly, there are many ways to match the requirements. To simplify the design, the groups (K_1, K_2) can be determined at the same values for the first UWB response and the second UWB response. In this study, $K_1 = 0.25$ and $K_2 = 1$, as mapped in Figure 2a, are used and then the corresponding length ratio R_1 is found to be 0.7 and length ratio R_2 is found to slightly more than 0.9, where the passband frequency ratios of $f_{e1}/f_{o1} = 1.58$ and f_{o2}/f_{o1} greater than 4.64. The transmission zeros are calculated to be 5.2 GHz (TZ₃) by using (3a), and the transmission zeros are determined to be 6.1 GHz (TZ₅) and 12.2 GHz (TZ₆) by using (3b).

The second UWB BPF is designed and optimized using a full wave EM simulation [30] and the dimension parameters are: $L'_1 = 1.85$ mm, $L'_2 = 3.1$ mm, $L'_s = 6.95$ mm, $L'_c = 5.92$ mm, $W'_1 = 3.43$ mm, $W'_2 = 0.2$ mm, $W'_s = 0.2$ mm, $G'_1 = 0.2$ mm, $G'_2 = 0.15$ mm, $G'_3 = 0.15$ mm. Figure 7 displays the simulated results which have insertion loss $|S_{21}|$ of 0.67 dB return loss $|S_{11}|$ of 13.81 dB and 3-dB fractional bandwidth (FBW) = 53%. Three transmission zeros are also appeared near the passband to have a high band selectivity.

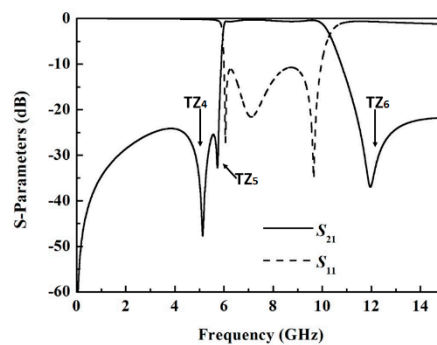


Figure 7. Simulated results of the second UWB BPF using EM simulation. For the second UWB BPF, $L_1' = 1.85$ mm, $L_2' = 3.1$ mm, $L_s' = 6.95$ mm, $L_c' = 5.92$ mm, $W_1' = 3.43$ mm, $W_2' = 0.2$ mm, $W_s' = 0.2$ mm, $G_1' = 0.2$ mm, $G_2' = 0.15$ mm, $G_3' = 0.15$ mm.

4.2. Measured Results

After designing the first UWB response and the second UWB response independently, they were combined together as shown in Figure 6, and the simulated results shown in Figure 8b include the individual response of the lower UWB shown in Figure 4 and higher UWB shown in Figure 7. The filter is also realized on the same commercial substrate (RT/Duroid 5880). Figure 8a displays the photograph of the fabricated BPF. The filter has length of $0.15 \lambda_g$ and width of $0.40 \lambda_g$, where λ_g is the guided wavelength at the first center frequency. The filter is fabricated and measured by an HP8510C Network Analyzer. Figure 8b displays simulated and measured results of the UWB BPF of the first UWB response from 3.1 to 5 GHz and second UWB response from 6 to 10.1 GHz. The measured results have average insertion loss $|S_{21}|$ of 1.3 dB, average return loss $|S_{11}|$ of 10 dB and 3-dB fractional bandwidth (FBW) = 52.1%, for the first UWB response; and average insertion loss $|S_{21}|$ of 1.15 dB, average return loss $|S_{11}|$ of 15 dB and 3-dB fractional bandwidth (FBW) = 55.7%, for the second UWB response. The transmission zeros appeared close the passband at 2.5 GHz (TZ₁), 2.95 GHz (TZ₂), 5.3 GHz (TZ₄), 6.2 GHz (TZ₃, TZ₅) and 11.3 GHz (TZ₆) to have a high band selectivity. The transmission zeros (TZ₃, TZ₅) are located at the same frequency and then overlapped. Measured group delays show an acceptable value varying from 0.2 ns to 1 ns. The proposed dual UWB BPF also has simple structure and good filter features, showing a good potential to be applied in UWB applications.

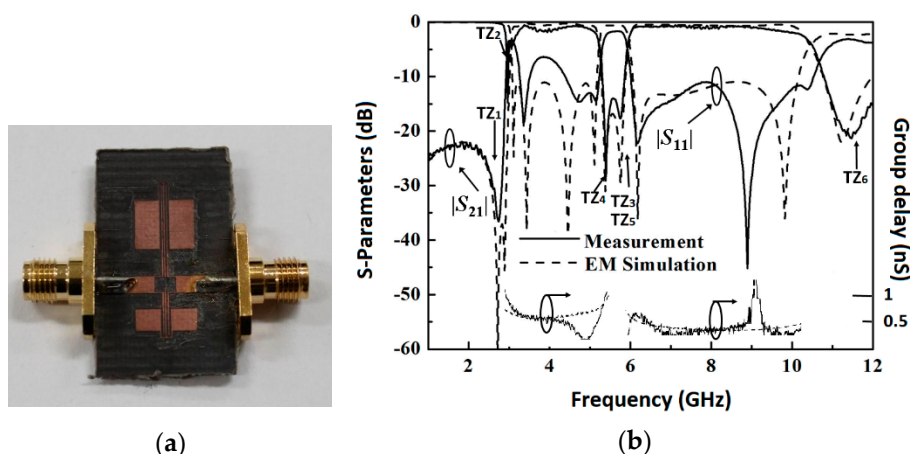


Figure 8. (a) Photograph and (b) simulated and measured results of the UWB BPF and group delay of the first UWB response from 3.1 to 5 GHz and second UWB response from 6 to 10.1 GHz. For the first UWB BPF, $L_1 = 3.35$ mm, $L_2 = 7.1$ mm, $L_s = 13.7$ mm, $W_1 = 3.38$ mm, $W_2 = 0.2$ mm, $W_s = 0.2$ mm, $G_1 = 0.2$ mm, $G_2 = 0.15$ mm, $G_3 = 0.15$ mm. For the second UWB BPF, $L_1' = 1.85$ mm, $L_2' = 3.1$ mm, $L_s' = 6.95$ mm, $W_1' = 3.43$ mm, $W_2' = 0.2$ mm, $W_s' = 0.2$ mm, $G_1' = 0.2$ mm, $G_2' = 0.15$ mm, $G_3' = 0.15$ mm.

Table 1 shows comparison of filter performances of the designed prototype with the previous published works, using parallel-coupled lines [10], asymmetric SIR [12], embedded open stubs [15], three pairs of coupled line sections with open-circuited stubs [23] and multi-layered substrate with two stub-loaded resonators [24]. This work has more transmission zeros and thus higher band selectivity than the conventional designs. Further, the fabricated dual-UWB BPF can be very compact. The measured results closely match the simulated results.

Table 1. Comparison of filter performances from this work with the previous published designs.

	Ref. [8]	Ref. [9]	Ref. [12]	Ref. [15]	Ref. [23]	Ref. [24]	This Work 1	This Work 2
Center frequency (GHz)	3.97	4/8	4	6.5	1	2.3	4.2	4.05/8.05
$ S_{11} $ (dB)	15	10/12	15	17	15	13	16.5	8/12
$ S_{21} $ (dB)	0.8	1.3/2.4	0.5	0.5	1.0	0.35	0.94	1.3/1.1
3-dB FBW (%)	45.3	42/58	62.5	113	123	80	52.7	52/55
Circuit size ($\lambda_g \times \lambda_g$)	0.66×0.43	0.70×0.28	1.12×0.1	0.4×0.06	0.17×0.14	0.53×0.43	0.15×0.25	0.15×0.4
Number of notched bands	0	1	0	1	0	2	0	1
Numbers of transmission zeros	2	2	3	0	1	1	3	5

5. Conclusions

This paper reported a stub-loaded stepped impedance resonator (SLSIR) and analyzed the even and odd resonant modes of this resonator using the input impedance/admittance analysis. For controlling the resonant modes of the SLSIR, two impedance ratios and two length ratios can be used as the design parameters. Several resonant mode variation curves were developed. Using resonant mode variation curves, resonant modes of the SLSIR can be tuned by the desired impedance ratios and length ratios to form different filtering types. In this paper, two types of the UWB BPFs were presented: a UWB filter with a wide stopband and a dual UWB filter (namely, a UWB with a notch band). The first odd mode and first even mode are selected to constitute an ultra-wideband, and the other odd mode and even mode are moved to higher frequencies. Moreover, since the input and output ports are set into the folded SLSIR, several transmission zeros are generated for the type of the resonator. The transmission zeros are generated for the coupling length between the coupled line with the resonator, and generated by the open stub. The transmission zeros are generated, improving the band selectivity of the designed filter using the SLSIR. The slight error of the band response is generated due to the substrate error. The simulation and measurement of the two designed cases are almost consistent, thus verifying the proposed design concepts.

Author Contributions: M.-H.W. contributed the design concept and wrote the paper, F.-Z.Z. and H.-Z.L. simulated, fabricated and measured the filter, and S.-K.L. provided the design resource and advised on the design procedure. All authors have read and agreed to the published version of the manuscript.

Funding: This research received no external funding.

Conflicts of Interest: The authors declare no conflict of interest.

References

1. US Federal Communications Commission. Revision of Part 15 of the Commission's Rules Regarding Ultra-Wideband Transmission Systems. In *First Report and Order, ET Docket*; Federal Communications Commission: Washington, DC, USA, 2002.
2. Weng, M.H.; Liu, S.K.; Liu, Y.T.; Hung, C.Y. A low loss ring UWB bandpass filter. *Microw. Opt. Tech. Lett.* **2008**, *50*, 2317–2319. [[CrossRef](#)]

3. Kim, C.H.; Chang, K. Ultra-wideband (UWB) ring resonator bandpass filter with a notched band. *IEEE Microw. Wirel. Compon. Lett.* **2011**, *21*, 206–208. [[CrossRef](#)]
4. Lan, S.W.; Weng, M.H.; Hung, C.Y.; Chang, S.J. Design of a compact ultra-wideband bandpass filter with an extremely broad stopband region. *IEEE Microw. Wireless Compon. Lett.* **2016**, *26*, 392–394. [[CrossRef](#)]
5. Wang, H.; Kang, W.; Miao, C.; Wu, W. Cross-shaped UWB bandpass filter with sharp skirt and notched band. *Electron. Lett.* **2012**, *48*, 96–97. [[CrossRef](#)]
6. Lee, J.K.; Kim, Y.S. Ultra-wideband bandpass filter with improved upper stopband performance using defected ground structure. *IEEE Microw. Wirel. Compon. Lett.* **2010**, *20*, 316–318. [[CrossRef](#)]
7. Song, Y.; Yang, G.M.; Geyi, W. Compact UWB bandpass filter with dual notched bands using defected ground structures. *IEEE Microw. Wirel. Compon. Lett.* **2014**, *24*, 230–232. [[CrossRef](#)]
8. Weng, M.H.; Huang, C.Y.; Hung, C.Y.; Lan, S.W. Design of an ultra-wideband bandpass filter by using coupled three line microstrip structure. *J. Electromagn. Waves Appl.* **2012**, *26*, 716–728. [[CrossRef](#)]
9. Weng, M.H.; Hsu, C.W.; Lan, S.W.; Yang, R.Y. An ultra-wideband bandpass filter with a notch band and a wide upper bandstop performances. *Electronics* **2019**, *8*, 1316. [[CrossRef](#)]
10. Bojra, A.L.; Belenguer, A.; Cascon, J.; Esteban, H.; Boria, V.E. Wideband passband transmission line based on metamaterial-inspired CPW balanced cells. *IEEE Antenna Wirel. Propag. Lett.* **2011**, *10*, 1421–1424.
11. Hameed, M.; Xiao, G.; Najam, A.I.; Qiu, L.; Hameed, T. Quadruple-mode wideband bandpass filter with improved out-of-band rejection. *Electronics* **2019**, *8*, 300. [[CrossRef](#)]
12. Chang, Y.C.; Kao, C.H.; Weng, M.H.; Yang, R.Y. Design of compact wideband bandpass filter using asymmetric SIR with low loss, high selectivity and wide stopband. *IEEE Microw. Wirel. Compon. Lett.* **2008**, *18*, 770–772. [[CrossRef](#)]
13. Ghatak, R.; Sarkar, P.; Mishra, R.K.; Poddar, D.R. A compact UWB bandpass filter with embedded SIR as band notch structure. *IEEE Microw. Wirel. Compon. Lett.* **2011**, *21*, 261–263. [[CrossRef](#)]
14. Li, R.; Zhu, L. Compact UWB bandpass filter using stub-loaded multiple-mode resonator. *IEEE Microw. Wirel. Compon. Lett.* **2007**, *17*, 40–42. [[CrossRef](#)]
15. Weng, M.H.; Liauh, C.T.; Wu, H.W.; Vargas, S.R. An ultra-wideband bandpass filter with an embedded open-circuited stub structure to improve in-band performance. *IEEE Microw. Wirel. Compon. Lett.* **2009**, *19*, 146–148. [[CrossRef](#)]
16. Zhou, Y.; Yao, B.; Cao, C.; Deng, H.; He, X. Compact UWB bandpass filter using ring open stub loaded multiple-mode resonator. *Electron. Lett.* **2009**, *45*, 554–556. [[CrossRef](#)]
17. Chu, Q.X.; Tian, X.K. Design of UWB bandpass filter using stepped-impedance stub-loaded resonator. *IEEE Microw. Wirel. Compon. Lett.* **2010**, *20*, 501–503. [[CrossRef](#)]
18. Han, L.; Wu, K.; Zhang, X. Development of packaged ultrawideband bandpass filters. *IEEE Trans. Microw. Theory Tech.* **2010**, *58*, 20–228.
19. Nosrati, M.; Mirzaee, M. Compact wideband microstrip bandpass filter using quasi-spiral loaded multiple-mode resonator. *IEEE Microw. Wirel. Compon. Lett.* **2010**, *20*, 607–609. [[CrossRef](#)]
20. Tu, W.H. Sharp-rejection broadband microstrip bandpass filter using penta-mode resonator. *Electron. Lett.* **2010**, *46*, 772–773. [[CrossRef](#)]
21. Fan, J.; Zhan, D.; Jin, C.; Luo, J. Wideband microstrip bandpass filter based on quadruple mode ring resonator. *IEEE Microw. Wirel. Compon. Lett.* **2012**, *22*, 348–350. [[CrossRef](#)]
22. Kumar, S.; Gupta, R.D.; Parihar, M.S. Multiple band notched filter using C-shaped and E-shaped resonator for UWB applications. *IEEE Microw. Wirel. Compon. Lett.* **2016**, *26*, 340–342. [[CrossRef](#)]
23. Zhang, T.; Xiao, F.; Bao, J.; Tang, X.H. Compact ultra-wideband bandpass filter with good selectivity. *Electron. Lett.* **2016**, *52*, 210–212. [[CrossRef](#)]
24. Li, Y.; Choi, W.W.; Tam, K.W.; Zhu, L. Novel wideband bandpass filter with dual notched bands using stub-loaded resonators. *IEEE Microw. Wirel. Compon. Lett.* **2017**, *27*, 25–27.
25. Velázquez-Ahumada, M.D.C.; Martel-Villagr, J.; Medina, F.; Mesa, F. Application of stub loaded folded stepped impedance resonators to dual band filters. *Prog. Electromagn. Res.* **2010**, *102*, 107–124. [[CrossRef](#)]
26. Liu, S.K.; Zheng, F.-Z. A new compact tri-band bandpass filter using step impedance resonators with open stubs. *J. Electromagn. Waves Appl.* **2012**, *26*, 130–139. [[CrossRef](#)]
27. Makimoto, M.; Yamashita, S. Bandpass filter using parallel-coupling stripline stepped impedance resonators. *IEEE Trans. Microw. Theory Tech.* **1980**, *28*, 1413–1417. [[CrossRef](#)]
28. Pozar, D.M. *Microwave Engineering*, 2nd ed.; John Wiley & Sons, Inc.: Hoboken, NJ, USA, 1998.

29. Hong, J.S.; Lancaster, M.J. *Microstrip Filters for RF/Microwave Applications*; John Wiley & Sons, Inc.: Hoboken, NJ, USA, 2001.
30. Zeland Software, Inc. *IE3D Simulator*; Zeland Software, Inc.: Fremont, CA, USA, 2002.



© 2020 by the authors. Licensee MDPI, Basel, Switzerland. This article is an open access article distributed under the terms and conditions of the Creative Commons Attribution (CC BY) license (<http://creativecommons.org/licenses/by/4.0/>).